Optics and Lasers in Engineering 55 (2014) 99–104

Contents lists available at ScienceDirect

Optics and Lasers in Engineering

journal homepage: www.elsevier.com/locate/optlaseng

Phase error analysis and compensation considering ambient light for phase measuring profilometry

Ping Zhou [a], Xinran Liu [a,*], Yi He [b], Tongjing Zhu [a]

[a] School of Biological Science & Medical Engineering, Southeast University, Nanjing 210096, China
[b] Shenzhen Institutes of Advanced Technology, Chinese Academy of Sciences, Shenzhen 518055, China

ARTICLE INFO

Article history:
Received 16 July 2013
Received in revised form
21 September 2013
Accepted 28 October 2013
Available online 15 November 2013

Keywords:
Phase error compensation
Gamma model
Ambient light
Phase-shifting

ABSTRACT

The accuracy of phase measuring profilometry (PMP) system based on phase-shifting method is susceptible to gamma non-linearity of the projector–camera pair and uncertain ambient light inevitably. Although many researches on gamma model and phase error compensation methods have been implemented, the effect of ambient light is not explicit all along. In this paper, we perform theoretical analysis and experiments of phase error compensation taking account of both gamma non-linearity and uncertain ambient light. First of all, a mathematical phase error model is proposed to illustrate the reason of phase error generation in detail. We propose that the phase error is related not only to the gamma non-linearity of the projector–camera pair, but also to the ratio of intensity modulation to average intensity in the fringe patterns captured by the camera which is affected by the ambient light. Subsequently, an accurate phase error compensation algorithm is proposed based on the mathematical model, where the relationship between phase error and ambient light is illustrated. Experimental results with four-step phase-shifting PMP system show that the proposed algorithm can alleviate the phase error effectively even though the ambient light is considered.

1. Introduction

Phase-shifting based phase-measuring profilometry (PMP) is one of the most widely used approaches in non-contact 3D shape measurements for its fast speed, high reliability and high accuracy, including biomedical applications [1], human body shape measurement [2], reverse engineering [3], and quality control [4]. For phase-shifting methods, the ideal sinusoidal waveforms are commonly employed for non-ambiguous 3D reconstruction. A series of sinusoidal fringe patterns are projected onto the object surface and captured by the camera, where the phase is modulated by the object height distribution. Then, the phase distribution is calculated by analysis of the images. Thus the object shape is measured or reconstructed through phase unwrapping methods and system calibration techniques.

In practice, there are many error sources that lead to the deviation of the fringe patterns captured by the camera from ideal ones and introduce additional phase error inevitably. Generally, the nonlinear response of gamma distortion in the projector–camera pair and uncertain ambient light are considered as the dominant error sources. To improve the accuracy of PMP system, many researches have been extensively proposed on addressing the effects of gamma distortion and improving gamma model. However, up to date, the effect of ambient light is still not explicit, and most of the experiments are performed in low-illumination or dark rooms [5]. Zhang and Yau analyzed the camera image generation procedure and utilized a lookup table (LUT) to alleviate the phase error [6]. Since the nonlinearity of camera is ignored in their derivation, the ambient light is considered as an independent factor. Chen et al. proposed a phase error compensation method by using smoothing spline approximation (SSA) [7], whereas the procedure of their work is time-consuming. Pan et al. proposed an iterative method and simplified phase error to one-order [8]. This phase error model is too simple to compensate the phase error accurately. Hoang et al. presented an advanced technique which can retrieve phase from multiple optical interferograms containing intensity nonlinearity and arbitrary phase shifts [9].

Recently, the gamma model was a popular researching field. Liu et al. developed a mathematical gamma model to predict the distortion effects and established a model of the harmonic coefficients about the gamma value [10]. They considered nonlinear response of both camera and projector as a combined gamma value for the projector–camera pair. Hoang et al. proposed a gamma correction method by applying a gamma pre-encoding process [11]. Li et al. incorporated the projector defocus into Liu's model and proposed a more accurate method to calibrate system gamma value [12]. Zhang et al. improved Liu's [10] and Li's [12] work and established a universal gamma model [13]. They employed gamma pre-encoding method to eliminate

* Corresponding author. Tel.: +86 15895950677; fax: +86 25 83790605.
E-mail address: xinranl425@gmail.com (X. Liu).

0143-8166/$ - see front matter © 2013 Elsevier Ltd. All rights reserved.
http://dx.doi.org/10.1016/j.optlaseng.2013.10.027

the phase error. Since the ambient light intensity is not considered in Liu's work [10], the effect of ambient light is neglected spontaneously in the subsequent gamma correction model [13]. Zhang and Yau proposed a method to measure objects with a high variation range of surface reflectivity, by taking a sequence of fringe images with different exposures [14]. Their approach may be useful for high dynamic range scanning, but it still requires a dark environment. Waddington et al. did some research to diminish the RMS errors for variable ambient illuminance [15,16]. Their work presented a method by adjusting the maximum input gray level to an optimal trade-off point. However, their method is short of mathematical gamma model with ambient light.

Considering the technical insufficiency of these protocols, in this paper, we performed theoretical analysis to phase error model taking account of both gamma non-linearity and ambient light. It is noteworthy that, a detailed mathematical gamma model to establish the relationship between the phase error and ambient light is proposed. Consequently, several experiments are implemented to demonstrate our model, in which the phase error is accurately compensated even in uncertain ambient lighting conditions.

2. Phase error analysis

2.1. Phase error model for PMP

Mathematically, the ideal intensity of the fringe pattern in a PMP system regardless of gamma nonlinearity is expressed as

$$I_{n,p} = A^p + B^p \cos(\phi^p + \delta_n) \tag{1}$$

where A^p and B^p are user defined constants, δ_n is $2\pi n/N$ that represents the phase-shifting value, n is the index and N is the phase-shifting total amount, $\phi^p = 2\pi f x$ is user defined phase information, f is the frequency, and x is the row coordinate of a pixel in projector. Although gamma distortion brings high-order harmonic inevitably in all PMP system and un-negligible ambient light brings additional phase error, the captured fringe pattern is still in the form of sinusoidal waveform generally when the gamma value and ambient light meet specific demands [8]. Therefore, the intensity of the captured fringe pattern could be expressed as

$$I^{\gamma}_{n,c} = \alpha[M + N \cos(\phi + \delta_n)]^{\gamma} \tag{2}$$

where the term α is a modulation constant controlling the intensity range, γ is the combined gamma value for the projector–camera pair, ϕ is the phase information corresponding to the desired object, M and N are normalized average intensity and intensity modulation respectively, which are related to the factors including reflectivity, uncertain ambient light, sensitive constant of the camera and gamma value of the projector. When the ambient light is not considered, the term M and N are equal to their initial values (0.5, in general) [10]. However, M and N may often vary as the ambient light exists in any case. Thus the actual phase derived from Eq. (2) should contain inevitable phase error related to the factors above.

To analyze the relationship between phase error and uncertain ambient light, we rewrite Eq. (2) as

$$I^{\gamma}_{n,c} = \alpha M^{\gamma}[1 + p \cos(\phi + \delta_n)]^{\gamma} \tag{3}$$

where $p = N/M$ is the ratio of intensity modulation to average intensity. Subsequently, the binomial series $(1+x)^t = \sum_{m=0}^{\infty} [(t/m)x^m]$ is applied to Eq. (3) whether gamma value is an integer or not, so that it is expressed as

$$I^{\gamma}_{n,c} = \alpha M^{\gamma} \sum_{m=0}^{\infty} \left[\binom{\gamma}{m} p^m \cos^m(\phi + \delta_n) \right] \tag{4}$$

According to the cosine power formulas, Eq. (4) can be expressed as

$$I^{\gamma}_{n,c} = A + \sum_{k=1}^{\infty} \{B_k \cos[k(\phi + \delta_n)]\} \tag{5}$$

$$B_k = 2M^{\gamma} \sum_{m=0}^{\infty} b_{k,m} \text{ and } A = 0.5B_0 \tag{6}$$

In addition,

$$b_{k,m} = (0.5p)^{2m+k} \binom{\gamma}{2m+k} \binom{2m+k}{m} \tag{7}$$

where k is a non-negative integer.

According to the binomial series, $B_k = 0$ when $k > \gamma$ if γ is an integer and $\gamma \geq 1$. On the contrary, B_k is a summation of infinite series if γ is not an integer, and the value of B_k is not divergent [10]. Fig. 1 shows the absolute value of B_k when $M = 0.5$, $\gamma = 2.2$, and $p = 1$, 0.8, and 0.6.

As shown in Fig. 1, B_k decreases dramatically with the increase of k no matter what the value of p is. The uppermost line describes the situation regardless of the ambient light where p maintains its initial value of 1 that is defined in most PMP systems generally. Furthermore, there is a noticeable difference when p is varied corresponding to varied ambient light.

To analyze the phase error model accurately, the harmonic waves up to the eighth-order are considered. For the four-step phase-shifting method (i.e., $n = 1$–4), the phase error can be derived from Eq. (5) as

$$\Delta\phi \approx -\arctan \frac{q \sin 4\phi - r \sin 4\phi + s \sin 8\phi}{1 + q \cos 4\phi + r \cos 4\phi + s \cos 8\phi} \tag{8}$$

where q, r, and s is B_3/B_1, B_5/B_1, and B_7/B_1 respectively. Writing the Taylor expansion of Eq. (8) around $q, r, s = 0$ we obtain

$$\Delta\phi \approx (-q + r + rs)\sin 4\phi + \left(\frac{q^2}{2} - \frac{r^2}{2} - s\right)\sin 8\phi + qs \sin 12\phi + \frac{s^2}{2} \sin 16\phi \tag{9}$$

Since $r \ll q$, $s \ll q$, the phase error has a simplified form if r and s are ignored.

$$\Delta\phi \approx -q \sin 4\phi + \frac{q^2}{2} \sin 8\phi \tag{10}$$

By setting $d\Delta\phi/d\phi = 0$, the maximum phase error of the four-step phase-shifting method can be derived as

$$\Delta\phi_{\max} = \frac{1}{16}\sqrt{(w+3)^3(w-1)} \tag{11}$$

where $w = \sqrt{8q^2 + 1}$.

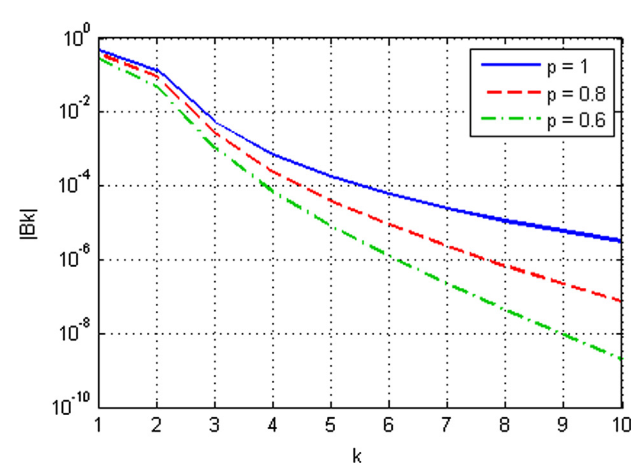

Fig. 1. The absolute values of B_k in different conditions.

We note that the phase error is determined by phase and the ratio q. Since the ratio q is related to ambient light according to the analysis from Eqs. (4) to (7), the effect of ambient light cannot be ignored.

2.2. Analysis of phase error and ambient light

Following Eq. (7), the ratio $b_{k+1,m}/b_{k,m}$ is derived as

$$\frac{b_{k+1,m}}{b_{k,m}} = \frac{p(\gamma-k-2m)}{2m+2k+2} \tag{12}$$

and it is equivalent to

$$2pmb_{k,m}+2mb_{k+1,m} = p(\gamma-k)b_{k,m}-2(k+1)b_{k+1,m} \tag{13}$$

similarly, we can derive Eq. (14) from Eq. (7).

$$2(m+1)b_{k,m+1}+2pmb_{k+1,m} = (\gamma-k-1)b_{k+1,m} \tag{14}$$

then, a formula named Eq. (15) can be obtained by summing Eqs. (13) and (14).

$$(\gamma+k+1)\hat{B}_{k+1} = p(\gamma-k)\hat{B}_k+2\left(\frac{1}{p}-p\right)C_k \tag{15}$$

with $\hat{B}_k = \sum_{m=0}^{\infty} b_{k,m}$ and $C_k = \sum_{m=0}^{\infty}(mb_{k,m})$.

Consequently, a recursive formula could be derived from Eq. (15) as

$$B_{k+1} = \frac{p(\gamma-k)}{\gamma+k+1}B_k+4M^{\gamma}\frac{1-p^2}{p(\gamma+k+1)}C_k \tag{16}$$

Therefore, q is derived as

$$q = q_1+q_2+q_3 \tag{17}$$

with

$$q_1 = \frac{p^2(\gamma-2)(\gamma-1)}{(\gamma+3)(\gamma+2)}, \quad q_2 = \frac{2(\gamma-2)(1-p^2)}{(\gamma+3)(\gamma+2)}\frac{C_1}{\hat{B}_1},$$
$$q_3 = \frac{2(1-p^2)}{p(\gamma+3)}\frac{C_2}{\hat{B}_1} \tag{18}$$

Fig. 2(a) shows the relationship between p and q, q_1, q_2, and q_3 in simulation, where gamma value is 2.4.

As shown in Fig. 2(a), the ratio q is related not only to the gamma value of projector–camera pair, but also to the ambient light which is corresponding to the ratio p. However, the calibration of system gamma is a complicated and time-consuming procedure. Moreover, the ratio p cannot be derived directly from the fringe patterns captured by the camera, so that an intermediate variable is defined as

$$t = \left(\frac{1-p}{1+p}\right)^{\gamma} = \left(\frac{M-N}{M+N}\right)^{\gamma} \tag{19}$$

the intermediate variable t could be derived from the entire white fringe pattern as $(M+N)^{\gamma}$ and the entire black fringe pattern as $(M-N)^{\gamma}$, where M and N are derived from their definition in Eq. (2). In that way, the ambient light can be quantified by the parameter t. Fig. 2(b) shows the relationship between t and q, q_1, q_2, and q_3 respectively, when gamma value is still 2.4.

In Fig. 2, we can see that q_1 always dominates the ratio q, and q_2, q_3 are tiny compared with the ratio q. Therefore, we introduced an approximate model to depict the relationship between the ratio q and ambient light parameter t, according to Eqs. (17)–(19), which does not require calibration of the system gamma.

$$q = a\left(\frac{1-t^b}{1+t^b}\right)^2+c \tag{20}$$

where a, b, and c are three coefficients.

According to Eqs. (10) and (20), the phase error will vary in different ambient light conditions. To compensate the phase error under a certain ambient light condition, the relationship described in Eq. (20) has to be calibrated.

3. Phase error compensation method

Following Hoang and Pan's theory, the phase error can be calculated by using a large number of phase-shifting fringe patterns [11]. For this reason, the sixteen-step phase-shifting fringe patterns and four-step fringe patterns are used in this paper to obtain the ideal phase and real phase, respectively. Subsequently, the phase error can be obtained by subtracting them.

To calibrate Eq. (20), the ambient light should be changed to different intensities. Two additional DLP projectors separated from the measurement system are used to simulate uniform and changeable ambient illuminance, just as those suggested by Waddington et al. [16]. The calibration has the following procedures:

1. The system projects the four-step and sixteen-step phase-shifting patterns onto a uniform flat surface in a certain ambient light condition. We calculate the phase error by using Hoang's method [11] and average the phase error at middle ten rows. Then the maximum phase error $\Delta\phi_{max}$ can be obtained easily, and q can be derived by using Eq. (11).
2. Additional entire white and black patterns are projected to obtain $(M+N)^{\gamma}$ and $(M-N)^{\gamma}$. Thus, for each pixel, $t(i,j)$ can be calculated based on its definition in Eq. (19). Also we average $t(i,j)$ at the middle ten rows to reduce random error and obtain $\bar{t}$.
3. By repeating the measurement in different ambient lighting conditions, Eq. (20) can be calibrated from at least eight pairs of q and $\bar{t}$. The coefficients a, b, and c can be obtained by using the least-square algorithm.

After Eq. (20) is calibrated, we can compensate the phase error for different ambient light conditions. When measuring objects

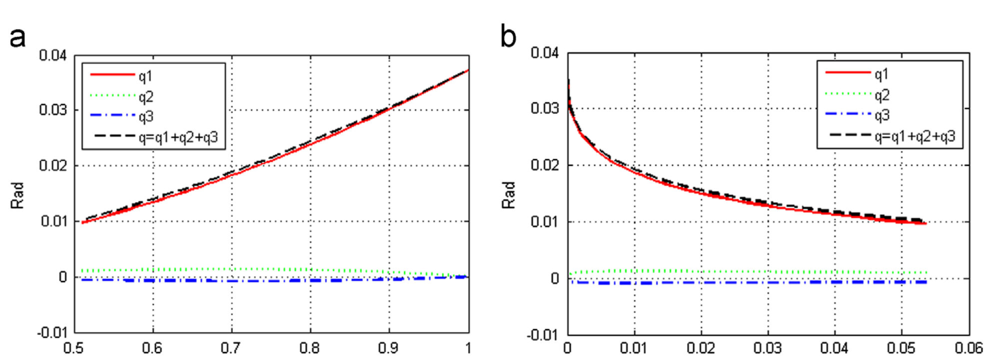

Fig. 2. Simulation results about the ratio q: (a) relationship between p and q, q_1, q_2, q_3; and (b) relationship between t and q, q_1, q_2, q_3.

under an unknown ambient light, additional entire white and black patterns are projected and captured to obtain $t(i, j)$. Then, $q(i, j)$ can be derived from the calibrated relationship. The phase error at (i, j) can be calculated based on Eq. (10), as expressed by

$$\Delta\phi(i,j) = -q(i,j)\sin 4[\phi(i,j)] + \frac{q(i,j)^2}{2}\sin 8[\phi(i,j)] \quad (21)$$

Therefore, the compensated phase is $\phi'(i,j) = \phi(i,j) - \Delta\phi(i,j)$.

4. Experiments and discussion

Our employed three-dimensional profile measurement system is composed of a BenQ GP1 projector and Microvision MVC-200UC camera.

Several experiments are performed to verify the phase error compensation model proposed in this paper. The four-step and sixteen-step phase-shifting fringe patterns are projected onto a flat board in two different ambient lighting conditions, so that the distorted phase value and ideal phase value could be derived respectively. The entire white and black patterns are also projected. The distorted phase error before compensation is shown in Fig. 3 (solid line). The phase error is tiny, because four-step phase-shifting algorithm is insensitive to even-order harmonic and the effect of gamma distortion is better than three-step phase-shifting case [17]. However, it is obvious that the amplitude of phase error is different corresponding to different ambient lighting conditions. The RMS error is 0.0252 rad in Figs. 3(a) and 0.0162 rad in Fig. 3(b). The experimental results agree with the analysis of the phase error model very well.

Following our phase error compensation method, eight pairs of q and $\bar{t}$ are obtained in different ambient lighting conditions, which are shown in Fig. 4. Specifically, saturation of camera sensor should be avoided when changing the ambient light, because the phase error will increase significantly when the camera is saturated and this error is not related to our model.

Subsequently, Eq. (20) is calibrated, which is expressed as Eq. (22) and is shown in Fig. 4.

$$q = 0.0497\left(\frac{1-t^{0.9556}}{1+t^{0.9556}}\right)^2 + 0.0011 \quad (22)$$

The value of coefficients a, b, and c might be different for each specific system. However, when the system properties, such as system gamma, lens aperture or exposure time of camera do not change, there is no need for recalibrating Eq. (20).

With the help of Eqs. (21) and (22), the phase error in unknown ambient light condition can be compensated simply and accurately by our method. The phase error after compensation is shown in Fig. 3 (dotted line). The RMS error reduces to 0.0019 and 0.0013 rad which is approximately 13 times smaller while the ambient light is considered.

In addition, even more complex objects are measured with our phase error compensation model, and one of experimental results of reconstructed faces is shown in the top of Fig. 5, and the central cross-section line of these faces to compare these results are shown in the bottom of Fig. 5. The experiment is performed in a certain ambient lighting condition. It can be seen that serious phase error exists before compensation in Fig. 5(a), which is caused by gamma distortion and ambient light. The RMS error of point cloud data is 0.0952 mm. In contrast, when the LUT method [6] is used, the phase error is alleviated to a certain level. However, there is still some minor phase error remaining in the reconstructed face with a RMS error of 0.0581 mm, as demonstrated in Fig. 5(b). This error is caused by the reason that the LUT method simply focuses on the gamma distortion of PMP system in a dark environment, which would not be suitable for the situation when the ambient light is involved. To achieve more accurate reconstructed face, the phase error compensation method proposed herein is used, and the experimental result is shown in Fig. 5(c). It is obvious that the reconstructed face after compensation is much smoother than that in Fig. 5(b) with well retained details. Correspondingly, the RMS error reduces to 0.0128 mm.

Fig. 6 shows a human hand that was measured under two different ambient light conditions. The captured images are shown in Fig. 6 (a) and (b). The ambient light condition in Fig. 6(a) is brighter than Fig. 6(b). The measured results before compensation are shown in Fig. 6(c) and (d) and the RMS errors are 0.0715 mm and 0.1140 mm, respectively. Fig. 6(e) and (f) shows the results after compensation with our proposed method. There is no obvious ripple on the surface, and the RMS errors are sharply reduced to 0.0120 mm and 0.0141 mm, respectively. These experimental results confirm that our proposed phase error compensation method can successfully improve the accuracy of PMP system in different ambient lighting conditions.

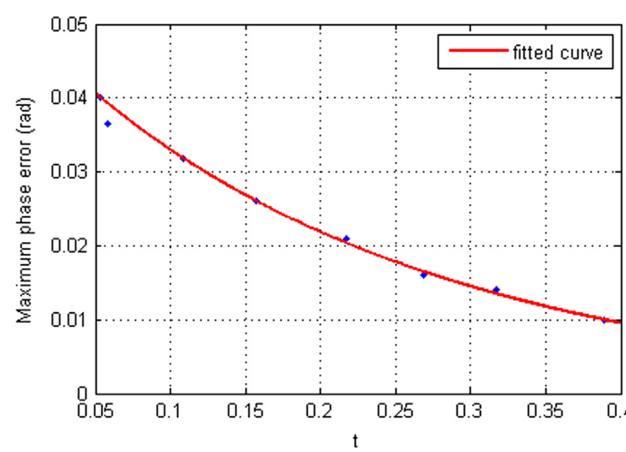

Fig. 4. The relationship between maximum phase error and t.

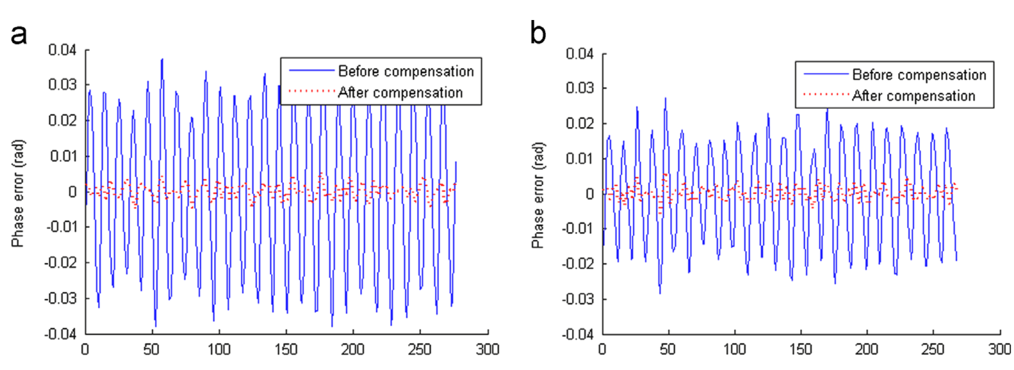

Fig. 3. Phase error compensation results of flat board in two ambient lighting conditions: (a) at dusk, and (b) in the afternoon.

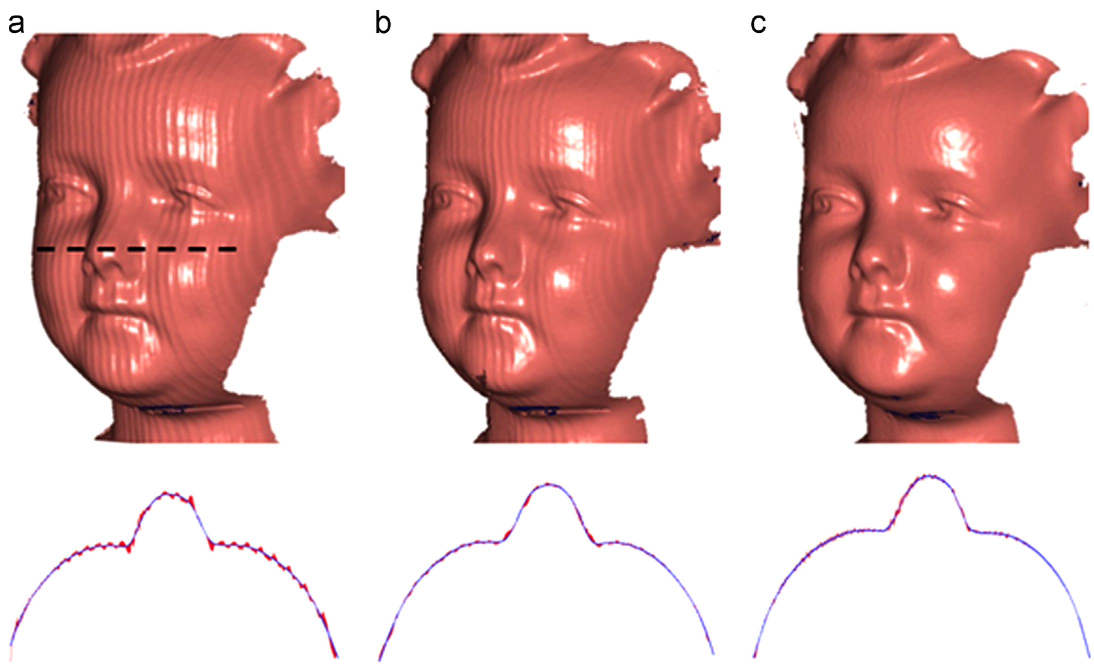

Fig. 5. Results of reconstructed faces and the cross sections with error plots: (a) before any compensation, (b) after compensation by LUT method, and (c) after compensation by our proposed method.

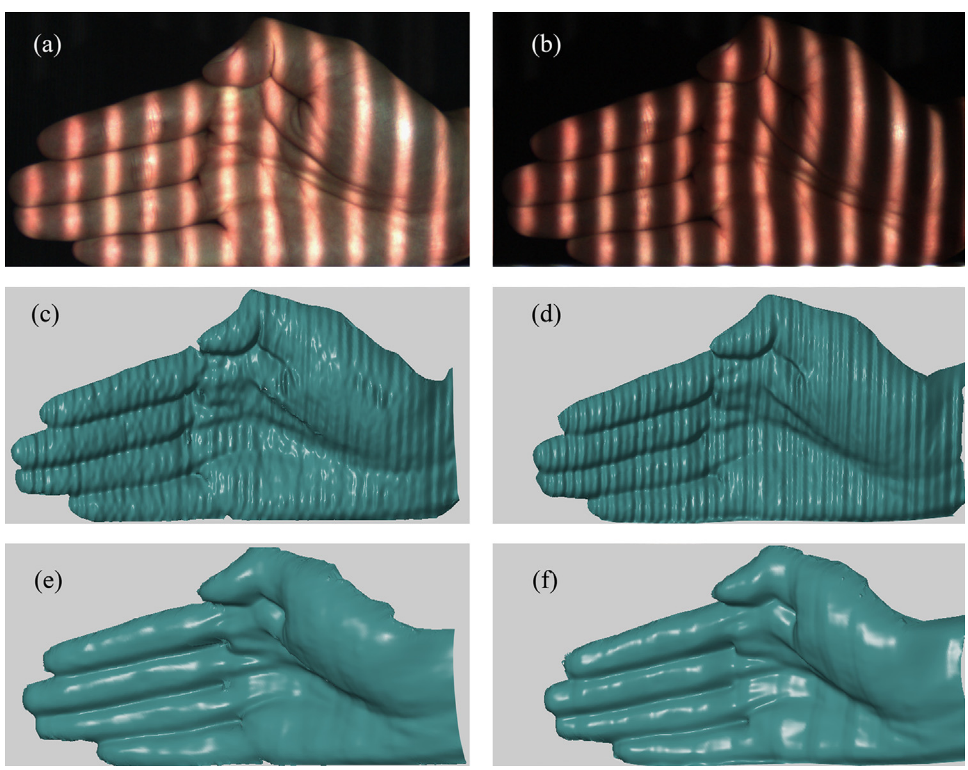

Fig. 6. Experimental results of human hand in two ambient light conditions: (a, b) captured images; 3D reconstruction results (c, d) before and (e, f) after compensation.

5. Conclusions

In this paper, we analyze the effects of ambient light on phase error compensation. It is confirmed theoretically and experimentally that the amplitude of phase error varies in different ambient lighting conditions. Based on this we develop a novel model to describe the relationship between ambient light and phase error. Subsequently, an accurate phase error compensation method is introduced to correct the phase error under any ambient lighting conditions. The experimental results show that the phase error can be reduced accurately in different ambient lighting conditions.

Acknowledgments

This work was supported by the National Nature Science Foundation of China (Grant NSFC 61127002) and Nature Science Foundation of Suzhou (Grant SYG201313).

References

[1] Chen L, Huang C. Miniaturized 3D surface profilometer using digital fringe projection. Meas Sci Technol 2005;16(5):1061–8.

[2] Lilley F, Lalor MJ, Burton DR. Robust fringe analysis system for human body shape measurement. Opt Eng 2000;39(1):187–95.

[3] Lin C, He H, Guo H, Chen M, Shi X, Yu T. Fringe projection measurement system in reverse engineering. J Shanghai Univ 2005;9(2):153–8.

[4] Yen H, Tsai D, Yang J. Full-field 3D measurement of solder pastes using LCD-based phase shifting techniques. IEEE Trans Electron Packag Manuf 2006;29(1):50–7.

[5] Dai M, Yang F, He X. Single-shot color fringe projection for three-dimensional shape measurement of objects with discontinuities. Appl Opt 2012;51(12):2062–9.

[6] Zhang S, Shing-Tung Y. Generic nonsinusoidal phase error correction for three-dimensional shape measurement using a digital video projector. Appl Opt 2007;46(1):36–43.

[7] Chen X, Xi J, Jin Y. Phase error compensation method using smoothing spline approximation for a three-dimensional shape measurement system based on gray-code and phase-shift light projection. Opt Eng 2008;47(11):19(113601).

[8] Pan B, Kemao Q, Huang L, Asundi A. Phase error analysis and compensation for nonsinusoidal waveforms in phase-shifting digital fringe projection profilometry. Opt Lett 2009;34(4):416–8.

[9] Hoang T, Wang Z, Vo M, Ma J, Luu L, Pan B. Phase extraction from optical interferograms in presence of intensity nonlinearity and arbitrary phase shifts. Appl Phys Lett 2011;99(3):031104.

[10] Liu K, Wang Y, Lau DL, Hao Q, Hassebrook LG. Gamma model and its analysis for phase measuring profilometry. J Opt Soc Am A: Opt Image Sci Vis 2010;27(3):553–62.

[11] Hoang T, Pan B, Nguyen D, Wang Z. Generic gamma correction for accuracy enhancement in fringe-projection profilometry. Opt Lett 2010;35(12):1992–4.

[12] Li Z, Li. Y. Gamma-distorted fringe image modeling and accurate gamma correction for fast phase measuring profilometry. Opt Lett 2011;36(2):154–6.

[13] Zhang X, Zhu L, Li Y, Tu D. Generic nonsinusoidal fringe model and gamma calibration in phase measuring profilometry. J Opt Soc Am A: Opt Image Sci Vis 2012;29(6):1047–58.

[14] Zhang S, Yau S. High dynamic range scanning technique. Opt Eng 2009;48(3):33604.

[15] Waddington C, Kofman J, Sinusoidal fringe-pattern projection for 3D surface measurement with variable illuminance. In: Proceedings of the international symposium on optomechatronic technologies. 2010, p. 1–5.

[16] Waddington C, Kofman J. Analysis of measurement sensitivity to illuminance and fringe-pattern gray levels for fringe-pattern projection adaptive to ambient lighting. Opt Laser Eng 2010;48(2):251–6.

[17] Vo M, Wang Z, Pan B, Pan T. Hyper-accurate flexible calibration technique for fringe-projection-based three-dimensional imaging. Opt Express 2012;20(15):16926–41.